RBFOX2 IS CRITICAL FOR MAINTAINING ALTERNATIVE POLYADENYLATION AND MITOCHONDRIAL HEALTH IN MYOBLASTS

Jun Cao[1], Elizabeth Jaworski[1], Kempaiah Rayavara[2], KarryAnne Belanger[1], Amanda Sooter[3], Sierra Miller[4], Sunil Verma[1], Ping Ji[1], Nathan Elrod[1], Eric J. Wagner[1,5], Vsevolod Popov[7], Nisha J. Garg[2], Andrew L. Routh[+1,5] and Muge N. Kuyumcu-Martinez[+1,4,6]

1 Department of Biochemistry and Molecular Biology, University of Texas Medical Branch, Galveston, Texas 2 Department of Microbiology and Immunology, University of Texas Medical Branch, Galveston, Texas

3 School of Medicine, University of Texas Medical Branch, Galveston, Texas

4 Institute for Translational Sciences, University of Texas Medical Branch, Galveston, Texas

5 Sealy Centre for Structural Biology and Molecular Biophysics, University of Texas Medical Branch, Galveston, Texas

6 Department of Neuroscience, Cell Biology, and Anatomy, Institute for Translational Sciences, Department of Neuroscience, Cell Biology, and Anatomy; University of Texas Medical Branch, Galveston, Texas

7 Department of Pathology, University of Texas Medical Branch, Galveston Texas

[+]Co-corresponding authors

Running title: Rbfox2 role in APA and mitochondria

Contact: Muge N. Kuyumcu-Martinez, nmmartin@utmb.edu, Department of Biochemistry and Molecular Biology; Institute for Translational Sciences; Department of Neuroscience, Cell Biology, and Anatomy, University of Texas Medical Branch, Galveston, Texas.

Andrew L. Routh, alrouth@utmb.edu, Department of Biochemistry and Molecular Biology; Sealy Centre for Structural Biology and Molecular Biophysics, University of Texas Medical Branch, Galveston, Texas.

ABSTRACT

The RNA binding protein RBFOX2 is linked to heart and skeletal muscle diseases; yet, RBFOX2-regulated RNA networks have not been systematically identified. Although RBFOX2 has a well-known function in alternative splicing (AS), it is unclear whether RBFOX2 has other roles in RNA metabolism that affect gene expression and function. Utilizing state of the art techniques Poly(A)-ClickSeq (PAC-seq) and nanopore cDNA sequencing, we revealed a new role for RBFOX2 in fine tuning alternative polyadenylation (APA) of pre-mRNAs in myoblasts. We found that depletion of RBFOX2 altered expression of mitochondrial genes. We identified the mitochondrial gene *Slc25a4* gene that transports ATP/ADP across inner mitochondrial membrane as a target of RBFOX2. Dissecting how RBFOX2 affects *Slc25a4* APA uncovered that RBFOX2 binding motifs near the distal polyadenylation site (PAS) are critical for expression of *Slc25a4*. Consistent with changes in expression of mitochondrial genes, loss of RBFOX2 altered mitochondrial membrane potential and induced mitochondrial swelling. Our results unveiled a novel role for RBFOX2 in maintaining APA decisions and expression of mitochondrial genes in myoblasts relevant to heart diseases.

Keywords: alternative polyadenylation/mitochondria/nanopore sequencing/

poly(A) sequencing/RBFOX2

Non-standard Abbreviations and Acronyms:

AS	alternative splicing
PAC-seq	poly(A)-ClickSeq
APA	alternative polyadenylation
KD	knock down
3´UTR	3´untranslated region
PAS	poly(A)-site
PAC	poly(A)-cluster
DPAC	differential-poly(A)-clustering
dPAS	distal poly(A)-site
pPAS	proximal poly(A)-site
ANT1 (*Slc25a4*)	ATP/ADP translocator (mitochondrial)
MFN1	Mitofusin

INTRODUCTION

The RNA binding protein RBFOX2 is critical for heart and skeletal muscle function. Loss of function mutations in *RBFOX2* are identified in patients with hypoplastic left heart syndrome (Homsy et al., 2015, Verma et al., 2016b). Low RBFOX2 activity is also associated with heart failure (Wei et al., 2015b) and cardiac complications of diabetes (Nutter et al., 2016, Nutter et al., 2017). *Rbfox2* ablation in mouse cardiomyocytes results in dilated cardiomyopathy and heart failure (Wei et al., 2015a). RBFOX2 is also important for skeletal muscle development and function (Singh et al., 2018, Singh et al., 2014). However, RBFOX2-regulated RNA networks necessary for muscle development and function have not been extensively defined. Thus, it still remains unclear how loss of RBFOX2 contributes to human heart and muscle diseases. Systematic identification of RBFOX2-regulated RNA networks is necessary to better understand its role in heart and muscle diseases.

Mitochondria are essential for heart and muscle function and mitochondrial functions diminish in human diseases including heart failure and diabetic hearts (Rosca and Hoppel, 2013). Mitochondrial defects are also implicated in congenital heart defects such as hypoplastic left heart syndrome (Karamanlidis et al., 2011), in which *RBFOX2* mutations have been identified (Homsy et al., 2015, Verma et al., 2016b). Although mitochondrial defects have been identified as a pathogenic contributor to the heart diseases in which RBFOX2 is implicated, it is unclear whether RBFOX2 is involved in mitochondrial function.

RBFOX2 has a well-characterized role in alternative splicing (AS) regulation of pre-mRNAs that can affect gene expression and function. RBFOX2 controls AS by

binding to a highly conserved motif (U)GCAUG in intronic and/or exonic regions of pre-mRNAs (Yeo et al., 2009, Huang et al., 2012, Sun et al., 2012, Lovci et al., 2013) and regulates AS in a large complex with other splicing regulators (Damianov et al., 2016). Due to its important role in AS, most focus has been on identification of RBFOX2-regulated AS events in heart and skeletal muscle (Runfola et al., 2015, Verma et al., 2016a, Singh et al., 2018). However, it is unknown whether RBFOX2 has additional roles in RNA processing that are important for muscle development and function. Recent studies have shown that RBFOX2 binds to the 3´UTR of transcripts close to poly(A) sites (PASs) (Wang et al., 2008, Weyn-Vanhentenryck et al., 2014, Lovci et al., 2013). The consequences of this binding are unknown and a role for RBFOX2 in cleavage and polyadenylation of pre-mRNAs has not yet been demonstrated.

Mammalian 3´end processing involves the cleavage of the pre-mRNA near the PAS followed by polyadenylation of the cleaved RNA. This process is complex and requires both *cis*-acting elements in the RNA and *trans*-acting proteins that bind to these elements and regulate cleavage and polyadenylation. Greater than 50% of genes in the human genome display more than one PASs and thus can generate multiple mRNA isoforms defined by different 3´ termini. Alternative polyadenylation (APA) is defined the differential usage of these PASs in a given mRNA, which can in turn regulate mRNA expression and homoeostasis (Derti et al., 2012). There are two major types of APA, namely splicing-APA and tandem-APA. Tandem-APA is mediated by the preferential usage of tandem PASs within the 3´UTR of the terminal exon. This type of APA can affect 3´UTR length and the presence of cis-acting regulatory motifs in the 3´UTR, modulating mRNA stability, localization or translation

(Di Giammartino et al., 2011). Splicing-APA, can lead to generation of multiple protein isoforms with distinct functions and properties via AS of the terminal exons that have PASs (Cooke et al., 1999). Tight regulation of APA is essential for normal growth and development and as a result aberrant APA has been linked to many disease states including heart failure, cancer, and muscle disease (Masamha et al., 2014, Creemers et al., 2016, Batra et al., 2014).

In this study, we investigated whether RBFOX2 influences APA decisions. We used long-read nanopore cDNA sequencing and Poly(A)-ClickSeq (PAC-seq) (Routh et al., 2017), which not only allowed precise and unbiased determination of APA but also the consequences of APA changes on gene expression and isoform generation. We identified 233 APA changes induced upon RBFOX2 depletion in H9c2 myoblasts (in short H9c2 cells), 43% of which exhibited mRNA level changes. Although RBFOX2 has a well-known role in splicing, to our surprise only 7% of all RBFOX2-induced APA changes exhibited splicing-APA. 91% of APA events showed tandem-APA changes, which affected 3´UTR length associated with changes in mRNA levels. Strikingly, loss of RBFOX2 resulted in increased mitochondrial membrane potential and mitochondrial swelling, adversely affecting mitochondrial health. Investigating the mechanism by which RBFOX2 regulates mitochondrial health revealed that RBFOX2 depletion altered mitochondrial gene expression. We found that RBFOX2 regulates APA of mitochondrial ATP/ADP translocator 1 (ANT1) gene *Slc25a4*. Our data demonstrate that RBFOX2 depletion affects APA usage in *Slc25a4* 3´UTR modulating its 3´UTR length and expression levels. Importantly, RBFOX2 binding motifs near the distal polyA site were critical in regulating expression of *Slc25a4* levels. In summary, we have identified a new

role for RBFOX2 in tuning APA patterns and mitochondrial health.

RESULTS

RBFOX2 depletion alters alternative polyadenylation patterns of genes in myoblasts

RBFOX2 binds to the 3´UTR of transcripts close to PASs but consequences are unknown (Wang et al., 2008, Weyn-Vanhentenryck et al., 2014, Lovci et al., 2013). PASs are important determinants of cleavage and polyadenylation of pre-mRNAs. The presence of more than one PASs can lead to APA of pre-mRNAs. Thus, we tested whether RBFOX2 has a role in APA regulation using H9c2 myoblasts. H9c2 myoblasts are clonal cells that were derived from rat embryonic heart tissue. We have previously shown that H9c2 cells can be used as a model system to study RBFOX2 function in RNA splicing as these myoblasts successfully recapitulated RBFOX2-mediated AS regulation of genes observed in mouse hearts (Nutter et al., 2016). We treated H9c2 cells with scrambled or *Rbfox2*-specific siRNAs and validated KD of RBFOX2 by Western blot (Fig. 1A). We isolated RNA from these cells and performed PAC-seq (Routh et al., 2017) and analyzed the data using the *DPAC* pipeline (Routh, 2019a). We detected 101,338 unique PASs with at least 5 unique reads mapping from at least one sample. Multiple PASs occurring within 10nts were clustered together to yield 81,035 unique PASs. We filtered out all PASs not mapping to 3´UTRs already annotated in the UCSC RefSeq database. 22,768 PASs were mapped to 10,964 unique mRNA transcripts, of which 5,317 contained multiple PASs and 556 contained multiple terminal exons (TE). With these criteria, DPAC reported a total of 593 individual PASs exhibiting

significant changes in abundance upon RBFOX2 KD (Fig. 1B). Importantly, these PAS changes resulted in 233 APA changes in RBFOX2 depleted cells (Fig. 1C, Data Supplement I). Gene Ontology biological function analysis of these APA events revealed genes involved in striated muscle development (Data Supplement II). This is consistent with RBFOX2's involvement in congenital heart defects (Homsy et al., 2015, Verma et al., 2016b) and muscle development (Singh et al., 2018, Singh et al., 2014).

We also investigated what types of APA were affected upon RBFOX2 depletion in H9c2 cells. Out of 233 APA events, 213 were tandem-APA, 17 were splicing-APA, and 3 displayed both splicing and tandem-APA (Fig. 1C). Our analysis of RBFOX2 KD cells identified *Slc6a8* gene, which has a role in muscle function, as one of the APA events that are altered in RBFOX2 KD cells. *Slc6a8* gene encodes for the sodium and chloride dependent creatine transporter and is necessary for energy metabolism by generating ATP from creatine. Loss of function mutations in this gene is associated with mental retardation and heart rhythm abnormalities (Anselm et al., 2008). *Slc6a8* has two PASs, one distal PAS (dPAS) and proximal PAS (pPAS) in H9c2 myoblasts. Upon RBFOX2 depletion, *Slc6a8* pPAS usage was increased (Fig. 1D, left panel). To validate the PAS usage in *Slc6a8* transcripts, we performed RT-qPCR using primers ("common") to detect total transcripts that are generated by both dPAS and pPAS usage and another primer pair ("distal") to amplify the longer transcripts produced by dPAS usage. The ratio of "distal" to "common" reflects the relative dPAS usage among all of the PASs. For *Slc6a8*, the ratio of distal to common transcripts was significantly decreased in RBFOX2 KD cells, suggesting that pPAS usage was increased in RBFOX2 KD cells consistent with the PAC-seq data (Fig. 1D, right panel vs left panel).

RBFOX2-mediated APA impacts 3´UTR length and mRNA levels

RBFOX2 depletion mainly altered tandem-APA (Fig. 1C), which can modulate the 3´UTR length and alter mRNA stability. Thus, we determined whether RBFOX2-mediated APA changes impact mRNA levels. Our DPAC pipeline identified 491 mRNA level changes (Fold Change > 1.5, p-adjust < 0.1) in RBFOX2 KD cells (Data Supplement III). RBFOX2 KD led to downregulation of 198 genes and upregulation of 293 genes (Fig. 2A). Gene ontology analysis (Kuleshov et al., 2016) of the 293 upregulated genes revealed categories including RNA splicing and RNA binding (Fig. 2B), as is an established function of RBFOX2 and may represent compensatory upregulation of proteins involved in these processes in response to RBFOX2 depletion. Conversely, analysis of the 198 downregulated genes (excluding RBFOX2) revealed that RBFOX2 KD impacts mitochondria specifically the mitochondrial membrane potential (Ψm) and mitochondrial respiratory chain complexes and ATP metabolic processes (Fig. 2B).

Analysis of PAC-seq data revealed that 59% (129 out of 216) APA changes led to 3´UTR shortening and 29.6% (64 out of 216) led to 3´UTR lengthening in RBFOX2 depleted cells (Fig. 2C). 23 genes that contained 3 or more PASs gave rise to complex changes resulting in transcripts that display both 3´UTR lengthening and shortening in RBFOX2 KD cells due to the modulation of levels of both the most distal and most proximal PASs relative to an intermediate PAS (Fig. 2C). With these criteria, *DPAC* reported that 99 out of 213 (46%) tandem-APA genes exhibited changes in mRNA expression levels (Fig. 2D).

To validate the tandem-APA changes that affect 3´UTR length and mRNA levels,

we used full-length cDNA by PCR followed by nanopore sequencing to determine the full-length transcripts with varying 3´UTR lengths in RBFOX2 KD H9c2 cells and compared these results to the PAC-seq data. We obtained high quality reads and read lengths using poly(A)-selected RNA from H9c2 cells using the MinION nanopore sequencer (Online Figure I). Full-length reads were mapped to the rn6 genome using *Minimap2* (Li, 2018) yielding ~310'000-740'000 mapped reads spanning 3000-4300 unique mRNAs, 190-413 of which had a coverage greater than 100 reads.

We analyzed APA of *Hdlbp* (high density lipoprotein binding protein gene), which was determined by PAC-seq to undergo 3´UTR shortening, and confirmed shortening by nanopore sequencing (Fig. 2E). There are 2 major PASs in *Hdlbp* 3´UTR as determined by PAC-seq (Fig. 2E, top panel). The usage of both of these PASs was confirmed by detection of both long and short *Hdlbp* transcripts by nanopore sequencing (Fig. 2E, bottom panel). In both sequencing strategies, dPAS usage was reduced (Fig. 2E, top panel) and shortened transcripts were predominant over lengthened transcripts in RBFOX2 KD cells (Fig. 2E, bottom panel). Nanopore sequencing is a powerful tool in defining full transcripts, exon connections (Bolisetty et al., 2015) and recombination events (Jaworski and Routh, 2017). Here, we provide strong evidence that nanopore can also be successfully used for validation of PAS usage and assessment of APA patterns. PAC-seq in parallel with nanopore sequencing determined RBFOX2-mediated tandem-APA usage and its effects on 3´UTR length and mRNA levels.

RBFOX2 depletion adversely impacted mitochondria health

Our results indicate that mitochondrial gene expression was downregulated in RBFOX2 KD cells (Fig. 2B). Mitochondrial function is essential for heart and skeletal muscle function and it declines in human heart failure and diabetic hearts (Rosca and Hoppel, 2013), in which RBFOX2 is implicated. In addition, mitochondrial defects have been identified in HLHS, in which *RBFOX2* mutations have been identified (Liu et al., 2017, Homsy et al., 2015, Karamanlidis et al., 2011).The role of RBFOX2 in mitochondrial function is unclear. Therefore, we investigated the status of mitochondria in RBFOX2 depleted cells.

Mitochondrial membrane potential is important for respiration and mitochondrion viability (Zorova et al., 2018). Therefore, we determined if RBFOX2 KD alters the mitochondrial membrane potential (Ψm), evaluated by the JC-1 dye assay. Mitochondrial membrane potential was increased by 2.5-fold in RBFOX2 KD (vs. control) cells (Fig. 3A). In response to rotenone (inhibits complex I), antimycin A (inhibits complex III), FCCP (mitochondrial oxidative phosphorylation uncoupler, depolarizes mitochondrial membrane potential), and H_2O_2 treatment, mitochondrial membrane potential was downregulated in both control and RBFOX2 KD cells; however, RBFOX2 KD cells maintained a higher baseline level of Ψm than was noted in control cells (Fig. 3A). These results suggest that increased mitochondrial membrane potential upon RBFOX2 deficiency could be an adaptive response to avoid mitochondrial release of electrons to oxygen and superoxide formation and subsequent reactive oxygen species induced oxidative injury to preserve basic cellular functions.

Mitochondrial fusion and fission play a key role in maintaining mitochondrial

health. Mitofusin 1 (MFN1) is an outer membrane GTPase that mediates mitochondrial clustering and fusion. Dynamin-like OPA1 protein regulates mitochondrial fusion and cristae structure in the inner mitochondrial membrane (Song et al., 2009). These two proteins together regulate the Ψm and electron transport chain function and are used as markers to assess electron transport chain function. Our immunofluorescence data showed that the MFN1 expression was not affected (Fig. 3B) whereas OPA1 protein level was modestly decreased with RBFOX2 depletion (Fig. 3C). Decreased expression of OPA1 protein was consistent with downregulation of its mRNA levels (1.2-fold) in RBFOX2 depleted H9c2 cells (Data Supplement III). To further determine the effect of RBFOX2 on mitochondrial health, we performed transmission electron microscopy to assess mitochondrial ultrastructure and morphology. We found that in RBFOX2 KD H9c2 cells, mitochondria were swollen as seen in representative micrographs (Fig. 3D), and also evident from increased mitochondrial area in RBFOX2-depleted cells (Fig. 3E). These type of morphological changes in mitochondria have been linked to rupture of mitochondria and apoptosis (Karbowski and Youle, 2003). Our findings indicate that RBFOX2 is important for mitochondrial health.

RBFOX2 regulates APA and expression levels of mitochondrial gene ATP/ADP translocase 1 (ANT1) gene (*Slc25a4*)

To better understand how RBFOX2 impacts mitochondrial health, we concentrated on mitochondrial genes regulated by an RBFOX2-dependent manner. *Slc25a4* gene encodes for ATP/ADP translocator critical for energy production in the mitochondria. It has been shown that ablation of mitochondrial gene *Slc25a4* (ANT1) in

mice causes cardiomyopathy associated with defects in mitochondrial respiration (Graham et al., 1997). Loss of function mutations in *Slc25a4* are linked to hypertrophic cardiomyopathy and skeletal muscle myopathy in humans (Korver-Keularts et al., 2015, King et al., 2018). *DPAC* analysis revealed that *Slc25a4* mRNA levels are downregulated by 1.63-fold (Data Supplement III). Moreover, *Slc25a4* undergoes a tandem-APA change in RBFOX2 KD cells. Therefore, we further assessed the regulation of *Slc25a4* via RBFOX2.

Slc25a4 has 2 major PASs in its 3´UTR. While distal PAS was minimally used in control cells, its usage was favored in RBFOX2 KD cells (Fig. 4A, top panel). This result from PAC-seq was validated by the presence of mostly long *Slc25a4* transcripts in low abundance in RBFOX2 KD H9c2 cells by nanopore sequencing (Fig. 4A, bottom panel).

To determine how RBFOX2 controls *Slc25a4* APA, we examined RBFOX2-Cross-Linking Immunoprecipitation (CLIP) seq data (ENCODE) and identified RBFOX2 binding sites within the 3´UTR of *Slc25a4* (Consortium, 2012, Davis et al., 2018). Examining the 3´UTR of rat *Slc25a4* revealed two RBFOX2 binding consensus binding sites 50-100nt away from dPAS of *Slc25a4* consistent with the CLIP-seq data (Fig. 4B). To determine the mechanism by which RBFOX2 controls *Slc25a4* expression, we tested whether RBFOX2 binding motifs near the distal PAS is important for *Slc25a4* expression. Therefore, we generated *Slc25a4* 3´UTR luciferase reporters. While generating these constructs we inserted parts of the *Slc25a4* 3´UTR downstream of the firefly luciferase ORF and removed the SV40 PAS within the plasmid (Fig. 4B). In this way, luciferase mRNA will be cleaved and polyadenylated using the PAS within the *Slc25a4* 3´UTR. We mutated two of the RBFOX2 “TGCATG” motifs near the distal PAS

and tested the relative luciferase activity of WT construct, and compared it to the mutant counterpart that disrupted the RBFOX2 binding consensus site. The mutation in RBFOX2 binding site led to increased relative luciferase activity (Fig. 4C). This is consistent with the finding that KD of RBFOX2 led to increased usage of this distal PAS (Fig. 4A vs 4C). Altogether, these results show that RBFOX2 binding motifs near the distal PAS are necessary for negative regulation of *Slc25a*4 expression.

RBFOX2 binding sites are enriched in the 3´UTRs near PASs that undergo APA changes in RBFOX2 depleted cells

Because RBFOX2 is critical in regulating *Slc25a4* APA and RBFOX2 binding sites are important for *Slc25a4* expression, we checked where the RBFOX2 binding sites are located with respect to all the PASs that are regulated by an RBFOX2-dependent manner. We performed metagene analysis using the available ENCODE RBFOX2-CLIP seq data (Consortium, 2012, Davis et al., 2018) and determined the distribution of RBFOX2 CLIP peaks 1000nt upstream and downstream of all PASs that were detected by PAC-seq in H9c2 cells as a control. Similarly, RBFOX2 binding sites were found both upstream and downstream of all PASs detected in H9c2 cells close to the PASs (labeled as position 0) (Fig. 5A, left panel). Notably, RBFOX2 binding site distribution was enriched within 250nt of the PASs undergoing APA changes in RBFOX2 KD cells by PAC-seq (Fig. 5A), suggesting that RBFOX2 binding may influence the PAS usage.

To validate RBFOX2 binding to the 3´UTRs of genes undergoing APA changes in RBFOX2 depleted cells, we performed an RNA pull down assay using *Rab7a* 3´UTR.

Ras related protein *Rab7a* undergoes APA changes in RBFOX2 KD cells (Fig. 5B). We validated RBFOX2-mediated PAS usage of *Rab7a* using RT-qPCR using specific primers (Online Table 2). For *Rab7a*, the ratio of "distal or long" to "common" transcripts was decreased in RBFOX2 KD cells, suggesting that pPAS usage was increased in RBFOX2 KD cells (Fig. 5B). Importantly, several RBFOX2 binding sites that span a large region (1kb) within the 3´UTR of *Rab7a* upstream of pPAS were identified using RBFOX2 CLIP-seq (ENCODE) (Consortium, 2012, Davis et al., 2018) (Fig. 5C). To determine whether RBFOX2 can bind *Rab7a* 3´UTR, we *in vitro* transcribed and biotinylated *Rab7a* RNA (584nt region of the 3´UTR) that includes the proximal PAC sequences and RBFOX2 binding sites. We mixed the RNA with protein lysates from uninduced or induced HEK293 cells. *Rab7a* 3´UTR pulled down FLAG-RBFOX2 only in induced cells expressing FLAG-RBFOX2 but not in uninduced cells (Fig. 5D), consistent with the identified RFBOX2 binding sites within *Rab7a* 3´UTR. Importantly, there was no non-specific binding of FLAG-RBFOX2 to the beads that lacked RNA (Fig. 5D, lane6 vs lane4). These data show that RBFOX2 is pulled down with the *Rab7a* 3´UTR that undergoes tandem-APA changes in RBFOX2 KD cells.

DISCUSSION

RBFOX2 is implicated in cardiovascular diseases, congenital heart defects and skeletal muscle development (Homsy et al., 2015, Verma et al., 2016b, Wei et al., 2015b, Nutter et al., 2016, Nutter et al., 2017, Sebastian et al., 2013, Singh et al., 2018a, Gallagher et al., 2011)). It is unclear whether RBFOX2 influences gene expression and function via other mechanisms besides AS. In this study, we addressed

this fundamentally important question utilizing state of the art techniques and performing functional assays. We uncovered a critical new role for RBFOX2 in maintaining APA patterns in myoblasts and provided insights into the functional consequences of APA changes mediated by RBFOX2 in myoblasts. In addition, our results revealed a novel role for RBFOX2 in regulating mitochondrial health relevant to human heart diseases.

In this study, combined usage of PAC-seq and nanopore sequencing allowed us to precisely determine RBFOX2-regulated APA patterns and evaluate the consequences of RBFOX2-mediated APA changes. PAC-seq allowed us to sensitively detect poly(A)-sites and simultaneously measure transcript abundance, while nanopore sequencing with MinION allowed us to validate PAS usage, simultaneously characterize exon inclusion across the entire mRNA transcript and determine 3´UTR length. By combining PAC-Seq and nanopore sequencing, we discovered a new role for RBFOX2 in APA regulation. We identified 233 APA changes in RBFOX2 KD myoblasts and found that 46% of these APA changes impacted mRNA levels. APA regulation is linked to physiological processes including heart development (Nimura et al., 2016), cell proliferation in immune response (Sandberg et al., 2008), and embryonic and postnatal development (Mangone et al., 2010). Aberrant regulation of APA is linked to pathological conditions including heart failure, cancer and muscular dystrophy (Masamha et al., 2014, Creemers et al., 2016, Batra et al., 2014).

AS can directly affect PAC usage and APA by regulating the splicing of exons that harbor PACs. RBFOX2 is a well-known regulator of AS. Despite its prominent role in AS, the majority of RBFOX2 induced APA changes were not mediated via splicing-APA. Instead, it was mediated via tandem-APA, which affected the length of 3´UTRs.

We were able to validate the 3´UTR length differences and tandem-APA induced by RBFOX2 using nanopore sequencing. Further dissection of how RBFOX2 influences APA patterns revealed that RBFOX2 binding sites near PASs are be an important determinant for APA decisions mediated by RBFOX2 in H9c2 cells. We used *Slc25a4* gene as a model to understand how RBFOX2 regulates APA and found that RBFOX2 binding sites near PASs are important determinants of PAS usage. Importantly, just mutating 2nt within RBFOX2 binding motifs increased gene expression, suggesting that RBFOX2 can act as a repressor of PAS usage when bound near the PASs. When we globally checked RBFOX2 binding sites with respect to PASs, we found that enrichment of RBFOX2 binding sites near PASs, suggesting that binding near PASs may be critical for APA decisions mediated by RBFOX2 in H9c2 cells.

In this study, we also focused on the functional consequences of RBFOX2-mediated gene expression changes. It has been known that RBFOX2 regulates AS of genes with roles in mitochondrial function (Yang et al., 2012, Hayakawa et al., 2002) but whether it affects mitochondria function was unclear. We found that RBFOX2 is critical in maintaining mitochondrial health. Importantly, we identified *Slc25a4* as a new APA target of RBFOX2. ANT1 is necessary for ATP/ADP translocation across the mitochondrial membrane during oxidative phosphorylation (Korver-Keularts et al., 2015, King et al., 2018). Mutations in this gene is linked to cardiomyopathy in human patients (Korver-Keularts et al., 2015, King et al., 2018). We found that RBFOX2 depletion affected *Slc25a*4 APA, and its expression levels. Consistently, both RBFOX2 deletion in cardiomyocytes and loss of *Slc25a*4 function resulted in dilated cardiomyopathy (Wei et al., 2015a, Korver-Keularts et al., 2015, King et al., 2018). Mitochondrial membrane

potential is important for ATP production, which is required for heart and muscle function and reduced mitochondrial function is a hallmark of failing hearts (Rosca and Hoppel, 2013). Importantly, we found profound changes in mitochondrial health upon RBFOX2 depletion. Finding a new role for RBFOX2 in mitochondrial function is highly relevant to its contribution to the development of heart diseases. Overall, our findings demonstrate that RBFOX2 controls mitochondrial gene *Slc25a4* via APA, providing novel insights into how RBFOX2 may alter mitochondrial health under diseased conditions.

MATERIALS AND METHODS

Cell culture

H9c2 cells (ATCC CRL-1446) were cultured and maintained in Dulbecco's modified Eagle's medium (DMEM) (ATCC 30-2002), supplemented with 10% fetal bovine serum (FBS, ATCC 30-2020), 100 units/ml penicillin and streptomycin (Thermofisher Scientific 15140122). Flag-tagged human RBFOX2^{WT} doxycycline induced Flp-in T-REx stable cells were generated as previously described (Belanger et al., 2019), and maintained in DMEM (Corning 10-013) supplemented with 10% tet-reduced FBS (Corning 35-075), 100units/ml penicillin and streptomycin (Thermofisher Scientific 15140122), 15µg/ml blasticidin (Corning 3513039), and 100ug/ml hygromycin (Corning, 30-240-CR). The stable cells were treated with 1 µg/ml doxycycline hyclate (Sigma D9891) for 24 hours to induce FLAG-RBFOX2 expression.

Transfections

For siRNA-KD experiments, H9c2 cells were seeded at 10^6 cells per 100mm dish and transfected with scrambled siRNA (Thermofisher Scientific AM4611) or *Rbfox2* siRNA (Thermofisher Scientific siRNA ID# s96620) at 20nM by Lipofectamine RNAiMAX (Thermofisher Scientific 13778150). Cells were harvested 72 hours post-transfection for RNA or protein extraction.

Confocal Immunofluorescence microscopy of mitochondrial proteins

H9C2 cells were seeded on to the Nunc lab-tek chamber slides for overnight and then fixed with 4% paraformaldehyde in PBS for 10 minutes followed by permeabilization and blocking in 0.1% triton X100 in 10% goat serum for 2 h. Cells were then incubated overnight with rabbit anti-OPA1 (Abcam ab157457) and mouse anti-MFN1 (Abcam ab57602) monoclonal antibodies, diluted in 10% goat serum. Then, cells were washed with PBS, incubated with Alexa Flour 594-conjugated goat anti-mouse or Alexa Flour 488-conjugated goat anti-rabbit secondary antibody, and slides were mounted using VECTASHIELD Antifade Mounting Medium with DAPI (Vector Laboratories, Burlingame, CA). Slides were imaged using Zeiss LSM 880 with Airyscan microscope with 63X 1.4 oil immersion objective and images were processed using Image J software.

Western Blot

Cells were lysed in lysis buffer (10mM HEPES-KOH, pH7.5, 0.32 M Sucrose, 5µM

MG132, 5mM EDTA, 1.0% SDS, and proteinase inhibitor cocktail from Roche) and sonicated. Protein concentration was determined by using the Bicinchoninic acid assay (BCA, Sigma BCA1-1KT). 30 µg of protein was separated on 10% SDS-PAGE and transferred to a PVDF membrane (Immobilon-P, Millipore). The membrane was blocked with 5% dry fat-free milk solution in PBS containing 0.1% Tween (PBST) at RT for 1 hour and then incubated with indicated primary antibodies overnight at 4°C. The membrane was washed with PBST for three times and incubated with HRP-conjugated secondary antibody for 1 hour at RT followed by three washes using PBST. Immobilon Western chemiluminescent (Millipore WBKLS0500) kit was used to detect HRP activity of the secondary antibody. The membrane was then imaged using ChemiDoc Touch imaging system (Bio-Rad). Image J software was used for band intensity quantification. Primary antibodies used for this study are as follows: RBFOX2 (1:1000, Abcam, ab57154), FLAG antibody (1:10000, Sigma, A8592) and α-tubulin (1:20000, Sigma-Aldrich, T6074).

RNA biotin pulldown assay

The 3´UTR sequence of *Rab7a* was amplified by RT-PCR using primers in Online Table S1 and cloned into pCRII-TOPO vector (Thermofisher Scientific K460001). The plasmid containing 3´UTR sequence was linearized by restriction digestion, gel purification and precipitation before *in vitro* transcription. Biotin labeled *Rab7a* RNA was generated by incorporation of 2µg linearized plasmid, 2µl mixed UTP containing 35% of Biotin-16-UTP (Sigma 11388908910) and 65% of 10mM UTP, 2µl 10mM ATP, 2µl 10mM GTP, 2µl 10mM CTP, 2µl 10X reaction buffer (Thermofisher Scientific AM1322) and 1µl SUPERase·In^{TM} RNase Inhibitor (Thermofisher Scientific AM2694) at 37°C for 1h. RNA

was precipitated and 4µg of biotinylated transcript was incubated with induced or uninduced Flp-in T-REx HEK293 stable cell lysates at 4°C for 1 h,which was followed by incubation with M280 magnetic streptavidin-coated beads (Thermofisher Scientific 11205D) at 4°C for 1 h. The beads washed 5 times in ice cold lysis buffer. RNA bound proteins were eluted by heating at 95°C for 5 minutes and detected by Western blot using specific antibodies.

JC-1 Mitochondrial membrane potential (Ψm) assay

H9c2 cells were seeded on to 96 well black flat bottom plates (Costar) and treated with siRNAs. After 24 hrs, cells were incubated in DMEM media without FBS and phenol red at 37 °C / 5% CO_2 with 5 µM rotenone (inhibits complex I) or 30 µM antimycin A (inhibits complex III) for 24 hrs. In some experiments, cells were also incubated with 250 µM mesoxalonitrile 4 – trifluoromethoxyphenylhydrazone (FCCP, uncoupler of membrane permeability and oxidative phosphorylation) or 400 µM H_2O_2 that was added during last 4 hrs of incubation. Plates were washed with PBS and then 100 µl of 10 µg/ml of JC-1 (5,5′,6,6′-tetrachloro-1,1′,3,3′-tetraethylbenzimidazolylcarbocyanine iodide, Invitrogen, T3168) added. Cells were incubated at 37 °C for 15 min in dark, washed twice with PBS, and 100 µl PBS was added to each well. Plates were read in SpectraMax M2 (Molecular Devices) to measure red J-aggregates fluorescence (a sensitive marker of Ψm) at an excitation of 535 nm and emission of 595 nm and green J-monomers fluorescence (indicator of disruption of ΔΨm) at an excitation of 485 nm and emission of 535 nm. Ratio of red/green fluorescence was calculated and plotted on the graph.

RNA preparation

RNA was extracted from cells using TRIzol (Thermofisher Scientific 15596-018) following the manufacturer's protocol with the exception that RNA was precipitated overnight at -70°C. For PAC-seq, the amount and quality of RNA were analyzed by using an Agilent bioanalyzer at the University of Texas Medical Branch Next-Generation Sequencing Core facility. For nanopore sequencing, poly(A)+ RNA was enriched by using magnetic mRNA isolation kit (New England biolabs S1550S).

Poly(A)-ClickSeq (PAC-seq)

The PAC-seq protocol was previously described (Routh et al., 2017). Three samples per treatment/biological condition were used for the PAC-seq analysis. Briefly, 2 µg of total RNA was used to synthesize cDNA through standard reverse transcription initiated by Illumina 4N_21T primer p7 and terminated by incorporation of azido-nucleotides (AzVTPs). Subsequently, the cDNA was cleaned by addition of RNase H (NEB) and purified through DNA Clean and Concentrator Kit (Zymo) before click-reaction, in which the 5' hexynyl- "click-adapter" p5 was click-ligated with azido-terminated cDNA in the presence of copper-TBTA (Lumiprobe) and Vitamin C. After DNA purification, the clicked cDNA was mixed with indexing primer, universal primer complementary to p7 and One Taq Standard Buffer Master Mix for PCR amplification. PAC-seq libraries were submitted for 1x150 single end sequencing yielding between 14 and 25 million reads per sample. The output data was processed and mapped to the *Rattus norvegicus* genome (rn6) and poly(A)-clusters (PACs) were generated using the DPAC pipeline (Routh, 2019b), designed for automated analysis and annotation of poly(A)-targeted

RNA-seq libraries such as PAC-seq.

DPAC analysis

DPAC (version 1.16) computational pipelines (Routh, 2019b) simultaneously compare mRNA levels and poly(A)-site cluster (PAC) usage preference. In the DPAC pipeline, PACs are defined as clusters of individual PASs that are found within 10nts of one another. PAC-seq measures changes in mRNA transcript levels uses DESeq2 (Love et al., 2014) with equivalent sensitivity to canonical randomly-primed RNA-seq approaches (Elrod et al., 2019). Differential gene expression is calculated by collapsing reads mapping to all PACs found within the same mRNA transcript (Elrod et al., 2019). *DPAC* measured changes in PAC usage between control and RBFOX2 KD cells. The differential PAC usage was reported if an individual PAC comprises at least 5% of a gene's PACs, has a fold change of >1.5, and results with an Independent Hypothesis Weighted (Ignatiadis et al., 2016) multiple testing p-adjusted value of < 0.1.

Nanopore sequencing with MinION

For nanopore sequencing, two sets of control and RBFOX2 KD H9c2 cells were used. Total cellular RNA was first poly(A) enriched and then amplified using oligo-dT primers and template switching oligos using Oxford Nanopore Technologies (ONT) cDNA-PCR sequencing kit (PCS108) as prescribed by the manufacturer. Samples were multiplexed using ONT barcodes. Pooled samples were sequenced on R9.4 flow cells. Reads were demultiplexed and base-called using Albacore followed by mapping to the rat genome

(rn6) using the –splice function of minimap2 (Li, 2016). Transcript isoforms were identified using FLAIR (Tang et al., 2018).

RT-qPCR

The RT-qPCR was conducted using LightCycler 480 Instrument (Roche) using the following conditions: 95 °C 10 s; 62 °C 15 s; 72 °C 10s for 40 cycles. Melting curve was obtained to ensure single product. ΔCt method was adopted for quantification. Primer sequences are provided in Online Table 1. *Hprt* was used as an internal control.

Metagene analysis

For metagene analysis, annotations for PACs identified in the rn6 genome were lifted over to the hg19 genome using the 'Lift Genome Annotations' tools on the UCSC Genome Browser. Coverage of eCLIP sites, assigning each BED entry with a score coverage of one, was generated both up and downstream by 1000nt relative to each PAC or for select PACs as indicated in the figures. Significant difference in BED coverage in different regions of the metagene were calculated using Mann-Whitey U test.

Transmission Electron Microscopy imaging of mitochondria

To obtain ultrastructural analysis of cells in ultrathin sections, cells were fixed for at least 1 hr in a mixture of 2.5% formaldehyde prepared from paraformaldehyde powder, and 0.1% glutaraldehyde in 0.05M cacodylate buffer pH 7.3 to which 0.01% picric acid and

0.03% $CaCl_2$ were added. Cell monolayers were washed in 0.1 M cacodylate buffer, were scraped off and processed further as a pellet. The pellets were post-fixed in 1% OsO_4 in 0.1M cacodylate buffer pH 7.3 for 1h, washed with distilled water and *en bloc* stained with 2% aqueous uranyl acetate for 20 min at 60^{o}C. The cell pellets were dehydrated in ethanol, processed through propylene oxide and embedded in Poly/Bed 812 (Polysciences, Warrington, PA). Ultrathin sections were cut on Leica EM UC7 ultramicrotome (Leica Microsystems, Buffalo Grove, IL), stained with lead citrate and examined in a JEM-1400 (JEOL USA, Peabody, MA) transmission electron microscope at 80 kV. Digital images were acquired with a bottom-mounted CCD camera Orius SC200 1 (Gatan, Pleasanton, CA).

Luciferase-3´UTR constructs

The 3´end of rat *Slc25a4* 3´UTR sequence which contains the distal poly(A) site (named as *Slc25a4* WT one pA) was cloned into pmirGLO Dual-luciferase vector (Promega, USA) downstream of firefly luciferase open reading frame (ORF). SV40 polyA site was removed in this plasmid to allow only the usage of the polyA site within the *Slc25a4* 3´UTR. Two RBFOX2 binding motifs near the distal poly(A) site in the 3´UTR of *Slc25a4* gene were abolished by mutating “CA” to “AC” (*Slc25a4* MUT one pA). 5X10^{5}/well of Flp-in T-REx 293 stable cells were seeded in 24 well plate 18h before transfection, and transfected with 100 ng DNA (*Slc25a4* 3´UTR constructs) per well with X-tremeGene 9 (Sigma Aldrich, USA). Cells were lysed 24h after transfection and luciferase activities were determined by Biotek plate reader Cytation 5 using the Dual luciferase assay kit (Promega, USA). Firefly luciferase was normalized to renilla luciferase activity and compared between WT and mutant

Slc25a4 constructs.

ACKNOWLEDGEMENTS

The authors acknowledge the University of Medical Branch Next Generation Sequencing Core Facility for providing RNA sequencing services. We thank the ENCODE Consortium and the ENCODE production laboratories generating the RBFOX2 eCLIP-seq datasets. We thank Dr. Ricardo Rajsbaum and Adam Hage for their help with the plate reader.

SOURCES OF FUNDING

This work was supported, in part, UTMB Department of Biochemistry and Molecular Biology Bridging funds; and a grant from the National Institutes of Health/ National Heart Lung Blood Institute [1R01HL135031] to M.N.K-M. The contents of the manuscript are solely the responsibility of the authors and do not necessarily represent the official views of NIH. J.C. is a funded by a post-doctoral fellowship from American Heart Association [18POST3399018]. N.J.G. is funded by grants from the National Institute of Allergy and Infectious Diseases [R01AI054578; R01AI136031] of the National Institutes of Health. A.R. is supported by start-up funds from UTMB. E.J.W. acknowledges support of BMB Startup funds and P.J is supported by funds from the National Institutes of Health [R03CA223893].

DISCLOURES

Authors declare no conflict of interest.

DATA AVAILABILITY AND ACCESSION NUMBERS

All raw sequencing data generated by Nanopore sequencing and PAC-Seq in this manuscript are deposited into the NCBI SRA database with project number PRJNA517125.

REFERENCES

ANSELM, I. A., COULTER, D. L. & DARRAS, B. T. 2008. Cardiac manifestations in a child with a novel mutation in creatine transporter gene SLC6A8. *Neurology,* 70**,** 1642-4.

BATRA, R., CHARIZANIS, K., MANCHANDA, M., MOHAN, A., LI, M., FINN, D. J., GOODWIN, M., ZHANG, C., SOBCZAK, K., THORNTON, C. A. & SWANSON, M. S. 2014. Loss of MBNL leads to disruption of developmentally regulated alternative polyadenylation in RNA-mediated disease. *Mol Cell,* 56**,** 311-322.

BELANGER, K., NUTTER, C. A., LI, J., YU, P. & KUYUMCU-MARTINEZ, M. N. 2019. A developmentally regulated spliced variant of PTBP1 is upregulated in type 1 diabetic hearts. *Biochem Biophys Res Commun,* 509**,** 384-389.

BOLISETTY, M. T., RAJADINAKARAN, G. & GRAVELEY, B. R. 2015. Determining exon connectivity in complex mRNAs by nanopore sequencing. *Genome Biol,* 16**,** 204.

CONSORTIUM, E. P. 2012. An integrated encyclopedia of DNA elements in the human genome. *Nature,* 489**,** 57-74.

COOKE, C., HANS, H. & ALWINE, J. C. 1999. Utilization of splicing elements and polyadenylation signal elements in the coupling of polyadenylation and last-intron removal. *Mol Cell Biol,* 19**,** 4971-9.

CREEMERS, E. E., BAWAZEER, A., UGALDE, A. P., VAN DEUTEKOM, H. W., VAN DER MADE, I., DE GROOT, N. E., ADRIAENS, M. E., COOK, S. A., BEZZINA, C. R., HUBNER, N., VAN DER VELDEN, J., ELKON, R., AGAMI, R. & PINTO, Y. M. 2016. Genome-Wide Polyadenylation Maps Reveal Dynamic mRNA 3'-End Formation in the Failing Human Heart. *Circ Res,* 118**,** 433-8.

DAMIANOV, A., YING, Y., LIN, C. H., LEE, J. A., TRAN, D., VASHISHT, A. A., BAHRAMI-SAMANI, E., XING, Y., MARTIN, K. C., WOHLSCHLEGEL, J. A. & BLACK, D. L. 2016. Rbfox Proteins Regulate Splicing as Part of a Large Multiprotein Complex LASR. *Cell,* 165**,** 606-19.

DAVIS, C. A., HITZ, B. C., SLOAN, C. A., CHAN, E. T., DAVIDSON, J. M., GABDANK, I., HILTON, J. A., JAIN, K., BAYMURADOV, U. K., NARAYANAN, A. K., ONATE, K. C., GRAHAM, K., MIYASATO, S. R., DRESZER, T. R., STRATTAN, J. S., JOLANKI, O., TANAKA, F. Y. & CHERRY, J. M. 2018. The Encyclopedia of DNA elements (ENCODE): data portal update. *Nucleic Acids Res,* 46**,** D794-D801.

DERTI, A., GARRETT-ENGELE, P., MACISAAC, K. D., STEVENS, R. C., SRIRAM, S., CHEN, R., ROHL, C. A., JOHNSON, J. M. & BABAK, T. 2012. A quantitative atlas of polyadenylation in five mammals. *Genome Res,* 22**,** 1173-83.

DI GIAMMARTINO, D. C., NISHIDA, K. & MANLEY, J. L. 2011. Mechanisms and consequences of alternative polyadenylation. *Mol Cell,* 43**,** 853-66.

ELROD, N. R., JAWORSKI, E. A., JI, P., WAGNER, E. J. & ROUTH, A. 2019. Development of Poly(A)-ClickSeq as a Tool Enabling Simultaneous Genome-wide Poly(A)-site identification and Differential Expression Analysis. *Methods*.

GRAHAM, B. H., WAYMIRE, K. G., COTTRELL, B., TROUNCE, I. A., MACGREGOR, G. R. & WALLACE, D. C. 1997. A mouse model for mitochondrial myopathy and

cardiomyopathy resulting from a deficiency in the heart/muscle isoform of the adenine nucleotide translocator. *Nat Genet,* 16**,** 226-34.

HAYAKAWA, M., SAKASHITA, E., UENO, E., TOMINAGA, S., HAMAMOTO, T., KAGAWA, Y. & ENDO, H. 2002. Muscle-specific exonic splicing silencer for exon exclusion in human ATP synthase gamma-subunit pre-mRNA. *J Biol Chem,* 277**,** 6974-84.

HOMSY, J., ZAIDI, S., SHEN, Y., WARE, J. S., SAMOCHA, K. E., KARCZEWSKI, K. J., DEPALMA, S. R., MCKEAN, D., WAKIMOTO, H., GORHAM, J., JIN, S. C., DEANFIELD, J., GIARDINI, A., PORTER, G. A., JR., KIM, R., BILGUVAR, K., LOPEZ-GIRALDEZ, F., TIKHONOVA, I., MANE, S., ROMANO-ADESMAN, A., QI, H., VARDARAJAN, B., MA, L., DALY, M., ROBERTS, A. E., RUSSELL, M. W., MITAL, S., NEWBURGER, J. W., GAYNOR, J. W., BREITBART, R. E., IOSSIFOV, I., RONEMUS, M., SANDERS, S. J., KALTMAN, J. R., SEIDMAN, J. G., BRUECKNER, M., GELB, B. D., GOLDMUNTZ, E., LIFTON, R. P., SEIDMAN, C. E. & CHUNG, W. K. 2015. De novo mutations in congenital heart disease with neurodevelopmental and other congenital anomalies. *Science,* 350**,** 1262-6.

HUANG, S. C., OU, A. C., PARK, J., YU, F., YU, B., LEE, A., YANG, G., ZHOU, A. & BENZ, E. J., JR. 2012. RBFOX2 promotes protein 4.1R exon 16 selection via U1 snRNP recruitment. *Mol Cell Biol,* 32**,** 513-26.

IGNATIADIS, N., KLAUS, B., ZAUGG, J. B. & HUBER, W. 2016. Data-driven hypothesis weighting increases detection power in genome-scale multiple testing. *Nat Methods,* 13**,** 577-80.

JAWORSKI, E. & ROUTH, A. 2017. Parallel ClickSeq and Nanopore sequencing elucidates the rapid evolution of defective-interfering RNAs in Flock House virus. *PLoS Pathog,* 13**,** e1006365.

KARAMANLIDIS, G., BAUTISTA-HERNANDEZ, V., FYNN-THOMPSON, F., DEL NIDO, P. & TIAN, R. 2011. Impaired mitochondrial biogenesis precedes heart failure in right ventricular hypertrophy in congenital heart disease. *Circ Heart Fail,* 4**,** 707-13.

KARBOWSKI, M. & YOULE, R. J. 2003. Dynamics of mitochondrial morphology in healthy cells and during apoptosis. *Cell Death Differ,* 10**,** 870-80.

KING, M. S., THOMPSON, K., HOPTON, S., HE, L., KUNJI, E. R. S., TAYLOR, R. W. & ORTIZ-GONZALEZ, X. R. 2018. Expanding the phenotype of de novo SLC25A4-linked mitochondrial disease to include mild myopathy. *Neurol Genet,* 4**,** e256.

KORVER-KEULARTS, I. M., DE VISSER, M., BAKKER, H. D., WANDERS, R. J., VANSENNE, F., SCHOLTE, H. R., DORLAND, L., NICOLAES, G. A., SPAAPEN, L. M., SMEETS, H. J., HENDRICKX, A. T. & VAN DEN BOSCH, B. J. 2015. Two Novel Mutations in the SLC25A4 Gene in a Patient with Mitochondrial Myopathy. *JIMD Rep,* 22**,** 39-45.

KULESHOV, M. V., JONES, M. R., ROUILLARD, A. D., FERNANDEZ, N. F., DUAN, Q., WANG, Z., KOPLEV, S., JENKINS, S. L., JAGODNIK, K. M., LACHMANN, A., MCDERMOTT, M. G., MONTEIRO, C. D., GUNDERSEN, G. W. & MA'AYAN, A. 2016. Enrichr: a comprehensive gene set enrichment analysis web server 2016 update. *Nucleic Acids Res,* 44**,** W90-7.

LI, H. 2016. Minimap and miniasm: fast mapping and de novo assembly for noisy long sequences. *Bioinformatics,* 32**,** 2103-10.

LI, H. 2018. Minimap2: pairwise alignment for nucleotide sequences. *Bioinformatics,* 34**,** 3094-3100.

LIU, X., YAGI, H., SAEED, S., BAIS, A. S., GABRIEL, G. C., CHEN, Z., PETERSON, K. A., LI, Y., SCHWARTZ, M. C., REYNOLDS, W. T., SAYDMOHAMMED, M., GIBBS, B., WU, Y., DEVINE, W., CHATTERJEE, B., KLENA, N. T., KOSTKA, D., DE MESY BENTLEY, K. L., GANAPATHIRAJU, M. K., DEXHEIMER, P., LEATHERBURY, L., KHALIFA, O., BHAGAT, A., ZAHID, M., PU, W., WATKINS, S., GROSSFELD, P., MURRAY, S. A., PORTER, G. A., JR., TSANG, M., MARTIN, L. J., BENSON, D. W., ARONOW, B. J. & LO, C. W. 2017. The complex genetics of hypoplastic left heart syndrome. *Nat Genet,* 49**,** 1152-1159.

LOVCI, M. T., GHANEM, D., MARR, H., ARNOLD, J., GEE, S., PARRA, M., LIANG, T. Y., STARK, T. J., GEHMAN, L. T., HOON, S., MASSIRER, K. B., PRATT, G. A., BLACK, D. L., GRAY, J. W., CONBOY, J. G. & YEO, G. W. 2013. Rbfox proteins regulate alternative mRNA splicing through evolutionarily conserved RNA bridges. *Nature Structural & Molecular Biology,* 20**,** 1434-1442.

LOVE, M. I., HUBER, W. & ANDERS, S. 2014. Moderated estimation of fold change and dispersion for RNA-seq data with DESeq2. *Genome Biol,* 15**,** 550.

MANGONE, M., MANOHARAN, A. P., THIERRY-MIEG, D., THIERRY-MIEG, J., HAN, T., MACKOWIAK, S. D., MIS, E., ZEGAR, C., GUTWEIN, M. R., KHIVANSARA, V., ATTIE, O., CHEN, K., SALEHI-ASHTIANI, K., VIDAL, M., HARKINS, T. T., BOUFFARD, P., SUZUKI, Y., SUGANO, S., KOHARA, Y., RAJEWSKY, N., PIANO, F., GUNSALUS, K. C. & KIM, J. K. 2010. The landscape of C. elegans 3'UTRs. *Science,* 329**,** 432-5.

MASAMHA, C. P., XIA, Z., YANG, J., ALBRECHT, T. R., LI, M., SHYU, A. B., LI, W. & WAGNER, E. J. 2014. CFIm25 links alternative polyadenylation to glioblastoma tumour suppression. *Nature,* 510**,** 412-6.

NIMURA, K., YAMAMOTO, M., TAKEICHI, M., SAGA, K., TAKAOKA, K., KAWAMURA, N., NITTA, H., NAGANO, H., ISHINO, S., TANAKA, T., SCHWARTZ, R. J., ABURATANI, H. & KANEDA, Y. 2016. Regulation of alternative polyadenylation by Nkx2-5 and Xrn2 during mouse heart development. *Elife,* 5.

NUTTER, C. A., JAWORSKI, E., VERMA, S. K., PEREZ-CARRASCO, Y. & KUYUMCU-MARTINEZ, M. N. 2017. Developmentally Regulated Alternative Splicing Is Perturbed in Type 1 Diabetic Skeletal Muscle. *Muscle & Nerve,* 56**,** 744-749.

NUTTER, C. A., JAWORSKI, E. A., VERMA, S. K., DESHMUKH, V., WANG, Q. L., BOTVINNIK, O. B., LOZANO, M. J., ABASS, I. J., IJAZ, T., BRASIER, A. R., GARG, N. J., WEHRENS, X. H. T., YEO, G. W. & KUYUMCU-MARTINEZ, M. N. 2016. Dysregulation of RBFOX2 Is an Early Event in Cardiac Pathogenesis of Diabetes. *Cell Reports,* 15**,** 2200-2213.

ROSCA, M. G. & HOPPEL, C. L. 2013. Mitochondrial dysfunction in heart failure. *Heart Fail Rev,* 18**,** 607-22.

ROUTH, A. 2019a. DPAC: A Tool for Differential Poly(A)-Cluster Usage from Poly(A)-Targeted RNAseq Data. *G3 (Bethesda),* 9**,** 1825-1830.

ROUTH, A., JI, P., JAWORSKI, E., XIA, Z., LI, W. & WAGNER, E. J. 2017. Poly(A)-ClickSeq: click-chemistry for next-generation 3-end sequencing without RNA enrichment or fragmentation. *Nucleic Acids Res,* 45**,** e112.

ROUTH, A. L. 2019b. DPAC: a tool for Differential Poly(A) Site usage from poly(A) targeted RNAseq data. *bioRxiv***,** 531590.

RUNFOLA, V., SEBASTIAN, S., DILWORTH, F. J. & GABELLINI, D. 2015. Rbfox proteins regulate tissue-specific alternative splicing of Mef2D required for muscle differentiation. *J Cell Sci,* 128**,** 631-7.

SANDBERG, R., NEILSON, J. R., SARMA, A., SHARP, P. A. & BURGE, C. B. 2008. Proliferating cells express mRNAs with shortened 3' untranslated regions and fewer microRNA target sites. *Science,* 320**,** 1643-7.

SINGH, R. K., KOLONIN, A. M., FIOROTTO, M. L. & COOPER, T. A. 2018. Rbfox-Splicing Factors Maintain Skeletal Muscle Mass by Regulating Calpain3 and Proteostasis. *Cell Rep,* 24**,** 197-208.

SINGH, R. K., XIA, Z., BLAND, C. S., KALSOTRA, A., SCAVUZZO, M. A., CURK, T., ULE, J., LI, W. & COOPER, T. A. 2014. Rbfox2-coordinated alternative splicing of Mef2d and Rock2 controls myoblast fusion during myogenesis. *Mol Cell,* 55**,** 592-603.

SONG, Z., GHOCHANI, M., MCCAFFERY, J. M., FREY, T. G. & CHAN, D. C. 2009. Mitofusins and OPA1 mediate sequential steps in mitochondrial membrane fusion. *Mol Biol Cell,* 20**,** 3525-32.

SUN, S., ZHANG, Z., FREGOSO, O. & KRAINER, A. R. 2012. Mechanisms of activation and repression by the alternative splicing factors RBFOX1/2. *RNA,* 18**,** 274-83.

TANG, A. D., SOULETTE, C. M., BAREN, M. J. V., HART, K., HRABETA-ROBINSON, E., WU, C. J. & BROOKS, A. N. 2018. Full-length transcript characterization of SF3B1 mutation in chronic lymphocytic leukemia reveals downregulation of retained introns. *bioRxiv***,** 410183.

VERMA, S. K., DESHMUKH, V., NUTTER, C. A., JAWORSKI, E., JIN, W., WADHWA, L., ABATA, J., RICCI, M., LINCOLN, J., MARTIN, J. F., YEO, G. W. & KUYUMCU-MARTINEZ, M. N. 2016a. Rbfox2 function in RNA metabolism is impaired in hypoplastic left heart syndrome patient hearts. *Sci Rep,* 6**,** 30896.

VERMA, S. K., DESHMUKH, V., NUTTER, C. A., JAWORSKI, E., JIN, W. H., WADHWA, L., ABATA, J., RICCI, M., LINCOLN, J., MARTIN, J. F., YEO, G. W. & KUYUMCU-MARTINEZ, M. N. 2016b. Rbfox2 function in RNA metabolism is impaired in hypoplastic left heart syndrome patient hearts. *Scientific Reports,* 6.

WANG, E. T., SANDBERG, R., LUO, S., KHREBTUKOVA, I., ZHANG, L., MAYR, C., KINGSMORE, S. F., SCHROTH, G. P. & BURGE, C. B. 2008. Alternative isoform regulation in human tissue transcriptomes. *Nature,* 456**,** 470-6.

WEI, C., QIU, J., ZHOU, Y., XUE, Y., HU, J., OUYANG, K., BANERJEE, I., ZHANG, C., CHEN, B., LI, H., CHEN, J., SONG, L. S. & FU, X. D. 2015a. Repression of the Central Splicing Regulator RBFox2 Is Functionally Linked to Pressure Overload-Induced Heart Failure. *Cell Rep,* 10**,** 1521-1533.

WEI, C. L., QIU, J. S., ZHOU, Y., XUE, Y. C., HU, J., OUYANG, K. F., BANERJEE, I., ZHANG, C. M., CHEN, B. Y., LI, H. R., CHEN, J., SONG, L. S. & FU, X. D. 2015b. Repression of the Central Splicing Regulator RBFox2 Is Functionally Linked to Pressure Overload-Induced Heart Failure. *Cell Reports,* 10**,** 1521-1533.

WEYN-VANHENTENRYCK, S. M., MELE, A., YAN, Q., SUN, S., FARNY, N., ZHANG, Z., XUE, C., HERRE, M., SILVER, P. A., ZHANG, M. Q., KRAINER, A. R.,

DARNELL, R. B. & ZHANG, C. 2014. HITS-CLIP and integrative modeling define the Rbfox splicing-regulatory network linked to brain development and autism. *Cell Rep,* 6**,** 1139-1152.

YANG, R. F., ZHAO, G. W., LIANG, S. T., ZHANG, Y., SUN, L. H., CHEN, H. Z. & LIU, D. P. 2012. Mitofilin regulates cytochrome c release during apoptosis by controlling mitochondrial cristae remodeling. *Biochem Biophys Res Commun,* 428**,** 93-8.

YEO, G. W., COUFAL, N. G., LIANG, T. Y., PENG, G. E., FU, X. D. & GAGE, F. H. 2009. An RNA code for the FOX2 splicing regulator revealed by mapping RNA-protein interactions in stem cells. *Nat Struct Mol Biol,* 16**,** 130-7.

ZOROVA, L. D., POPKOV, V. A., PLOTNIKOV, E. Y., SILACHEV, D. N., PEVZNER, I. B., JANKAUSKAS, S. S., BABENKO, V. A., ZOROV, S. D., BALAKIREVA, A. V., JUHASZOVA, M., SOLLOTT, S. J. & ZOROV, D. B. 2018. Mitochondrial membrane potential. *Anal Biochem,* 552**,** 50-59.

FIGURE LEGENDS

Figure 1. RBFOX2 depletion in H9c2 cells leads to altered poly(A) site usage determined by Poly(A)-ClickSeq (PAC-seq).

(A) A representative Western blot showing efficient knock down (KD) of RBFOX2 in H9c2 cells. Ponceau staining of total proteins was used to monitor even protein loading.

(B) The volcano plot of PAS changes in control (ctrl) versus (vs) RBFOX2 KD H9c2 cells. Significantly changed PASs (Fold Change > 1.5, pAdj < 0.1) are colored in red.

(C) The number of genes undergo tandem or splicing-APA in RBFOX2 KD H9c2 cells.

(D) Tandem-APA change in *Slc6a8* gene in control vs RBFOX2 KD H9c2 cells. The ratio of “distal or long” to “common” mRNA expression levels of *Slc6a8* by RT-qPCR in control cells was normalized to 1. Statistical significance was calculated using unpaired t-test to compare two different groups in three independent experiments (n=3). Data represent means ± SD. **p=0.0051.

Figure 2: RBFOX2-regulated tandem-APA modulates 3´UTR length and affects mRNA levels.

(A) The number of downregulated and upregulated genes in RBFOX2 KD H9c2 cells. **(B)** Gene ontology analysis of downregulated or upregulated genes in RBFOX2 depleted H9c2 cells.

(C) The number of genes undergoing tandem-APA generating shorter or longer 3´UTRs in RBFOX2 KD H9c2 cells.

(D) The number of genes that undergo both APA and mRNA level changes in RBFOX2 KD H9c2 cells.

(E) *Hdlbp 3´UTR* shortening mediated via tandem-APA in RBFOX2 depleted H9c2 cells identified by PAC-seq (top panel) or by nanopore sequencing (bottom panel).

Figure 3: RBFOX2 depletion in H9c2 cells affects mitochondrial health.

(A) Mitochondrial membrane potential (Δψm) was determined by JC-1 staining of the H9c2 cells transfected with scrambled or *Rbfox2* siRNAs. Shown are the ratios of fluorescence intensity of J-aggregates (red fluorescence) to J-monomers (green fluorescence). Statistical significance was calculated using unpaired t-test to compare two different groups in five replicates of two independent experiments. Data represent means ± SD. For mitochondrial membrane potential in untreated control vs RBFOX2-KD H9c2 cells, ****p<0.0001; in control vs RBFOX2-KD H9c2 cells treated with Rotenone, ***p= 0.0004; in control vs RBFOX2-KD H9c2 cells treated with Antimycin A, ***p= 0.0009; in control vs RBFOX2-KD H9c2 cells treated with FCCP, **p= 0.0017; in control vs RBFOX2-KD H9c2 cells treated with H_2O_2, ****p<0.0001.

Immunoflourescence of mitochondrial markers. **(B)** MFN1 and **(C)** OPA1 in RBFOX2 KD H9c2 cells determined by confocal microscopy.

(D) Representative transmission electron microscopy images of mitochondria in control vs RBFOX2-KD H9c2 cells.

(E) The surface area of mitochondria in control and RBFOX2 depleted cells was calculated using Image J. Total of 229 mitochondrial were counted for each treatment.

Figure 4. RBFOX2 regulates 3´UTR length and expression of mitochondrial gene *Slc25a4*.

(A) *Slc25a4* 3´UTR lengthening mediated via tandem-APA in RBFOX2 depleted H9c2 cells identified by PAC-seq (top panel) or by nanopore sequencing (bottom panel).

(B) Cartoon representation of Luciferase-*Slc25a4* 3´UTR constructs with or without mutated RBFOX2 binding sites.

(C) Relative firefly luciferase levels in HEK293 cells expressing WT or RBFOX2 binding site mutant poly(A) (pA) Luciferase-*Slc25a4* 3´UTR constructs.

Figure 5. RBFOX2 binding sites are enriched upstream of poly(A) sites in 3´UTRs that undergo APA changes.

(A) Metagene analysis of RBFOX2 CLIP-binding distribution with respect to PASs in all detectable PASs, or in upregulated/downregulated PASs identified in RBFOX2 KD H9c2 cells.

(B) Genome browser image of *Rab7a* 3´UTR displays tandem-APA changes determined by PAC-seq (left). Tandem-APA change in *Rab7a* in control vs RBFOX2 KD H9c2 cells determined by RT-qPCR (right). The ratio of “distal or long” to “common” mRNA expression levels of *Rab7a* by RT-qPCR in control cells was normalized to 1. Statistical significance was calculated using unpaired t-test to compare two different groups in three independent experiments (n=3). Data represent means ± SD. *p=0.0466.

(C) RBFOX2 CLIP-seq reads mapped to the *Rab7a* 3´UTR.

(D) FLAG western blot of FLAG-RBFOX2 pulled down with *in-vitro* transcribed and biotinylated *Rab7a* transcripts in induced or uninduced HEK293 cells. No RNA was used as a negative control for non-specific protein binding in induced or uninduced cells.

Figure1

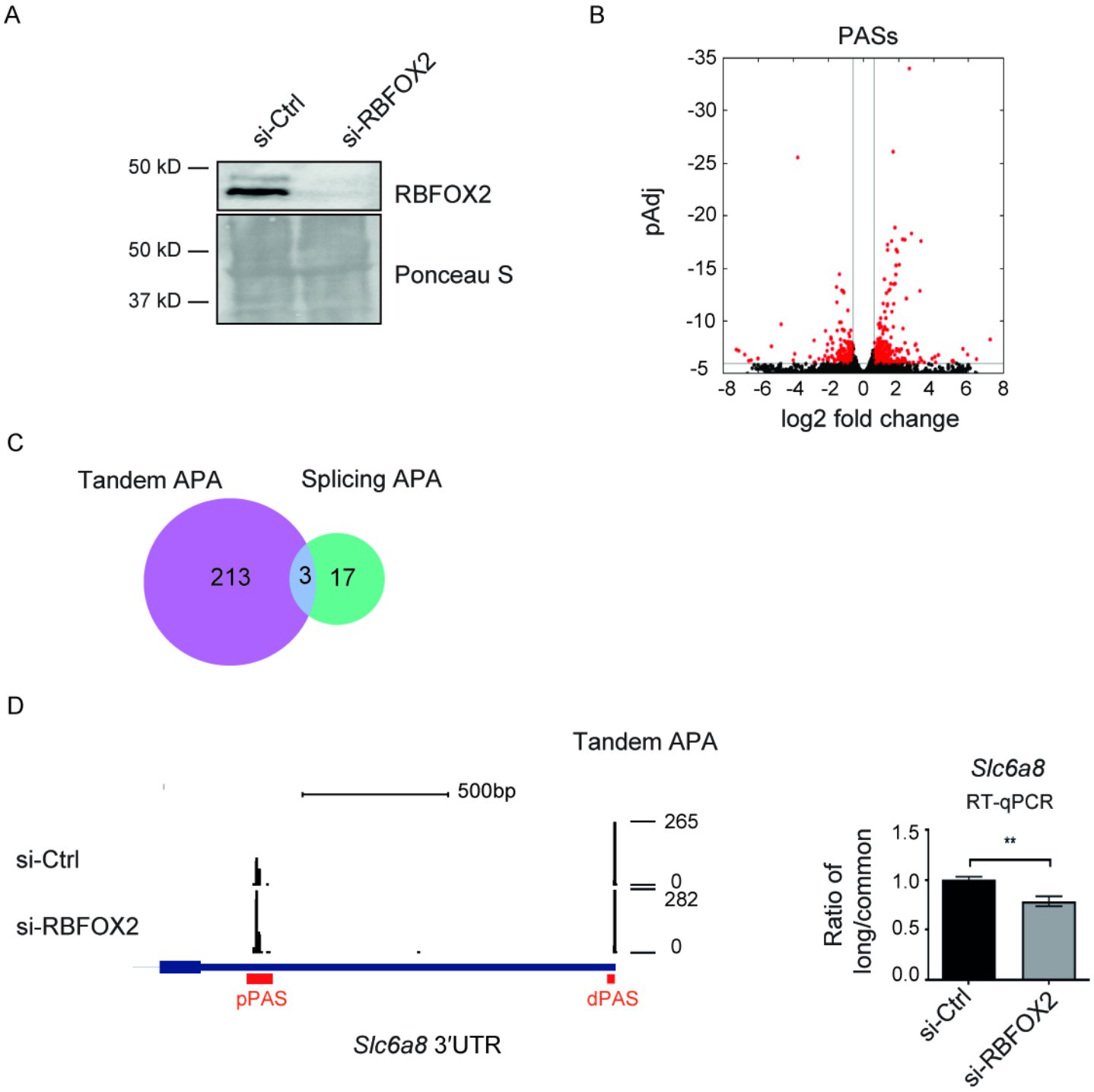

A

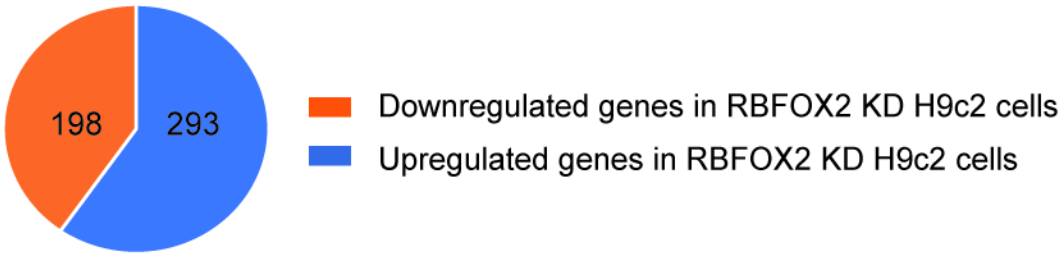

B

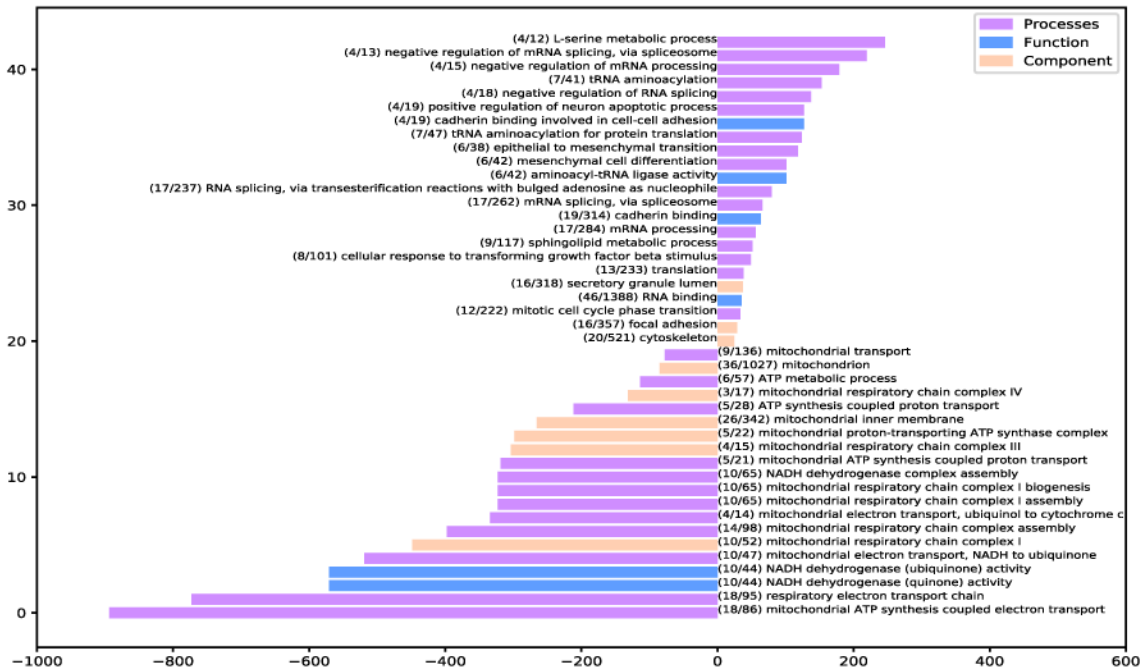

C

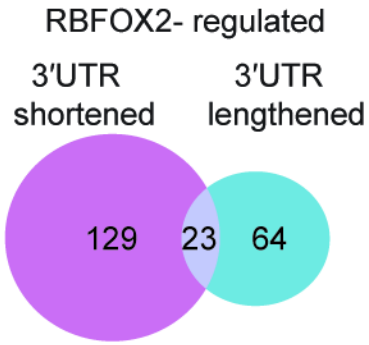

D

E

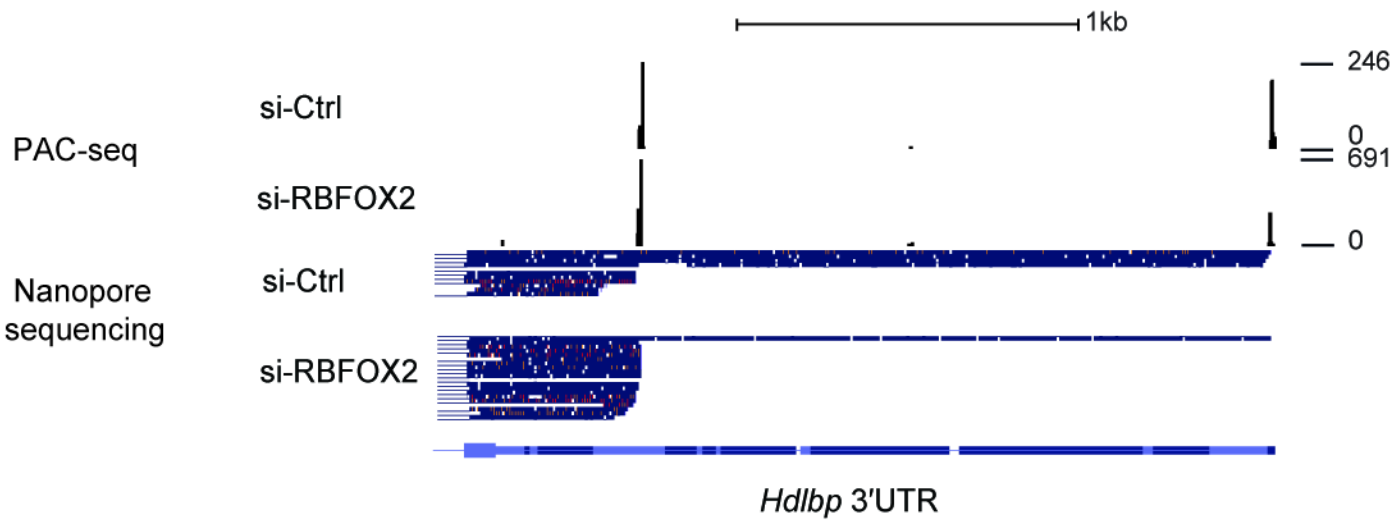

Figure 3

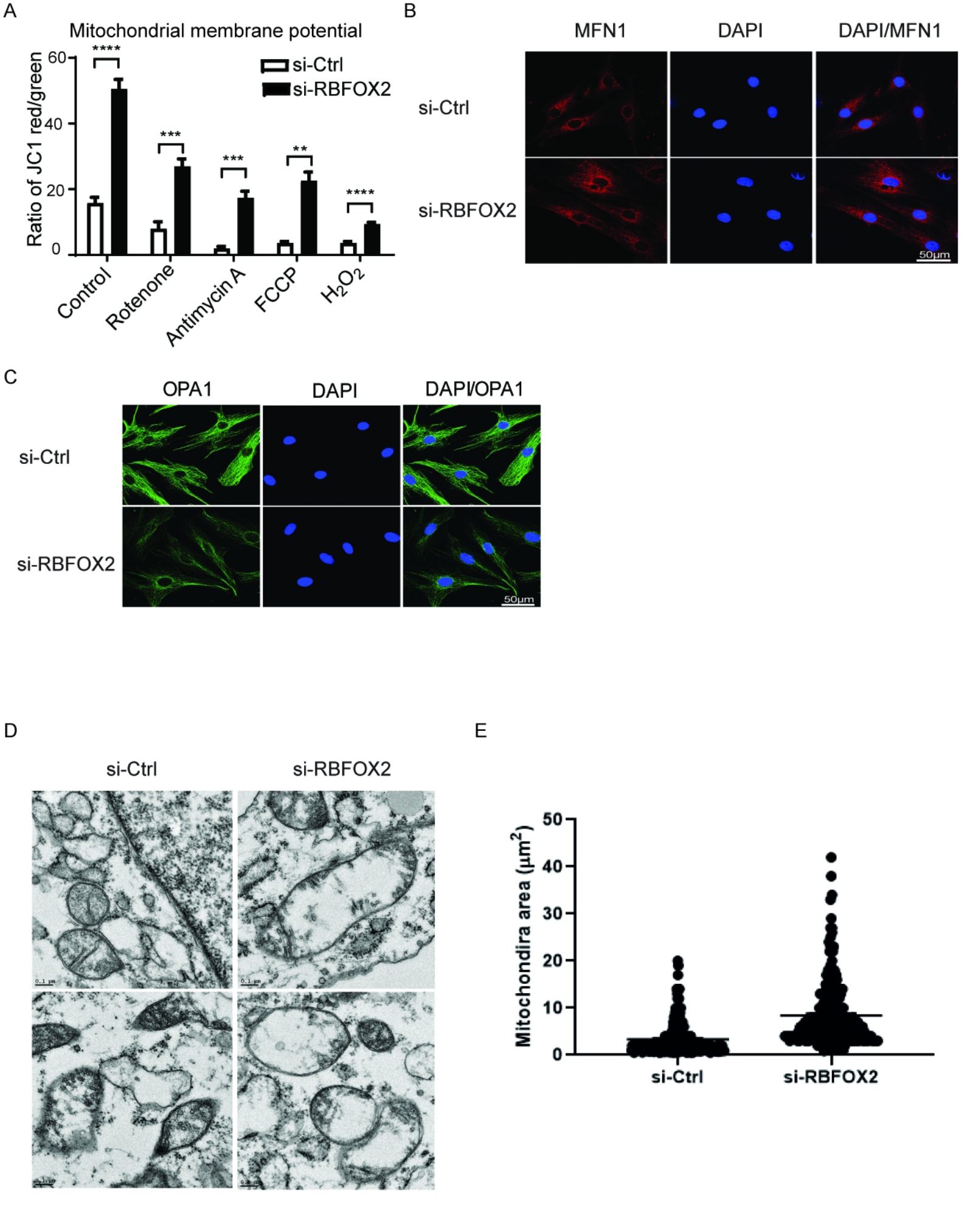

Figure4

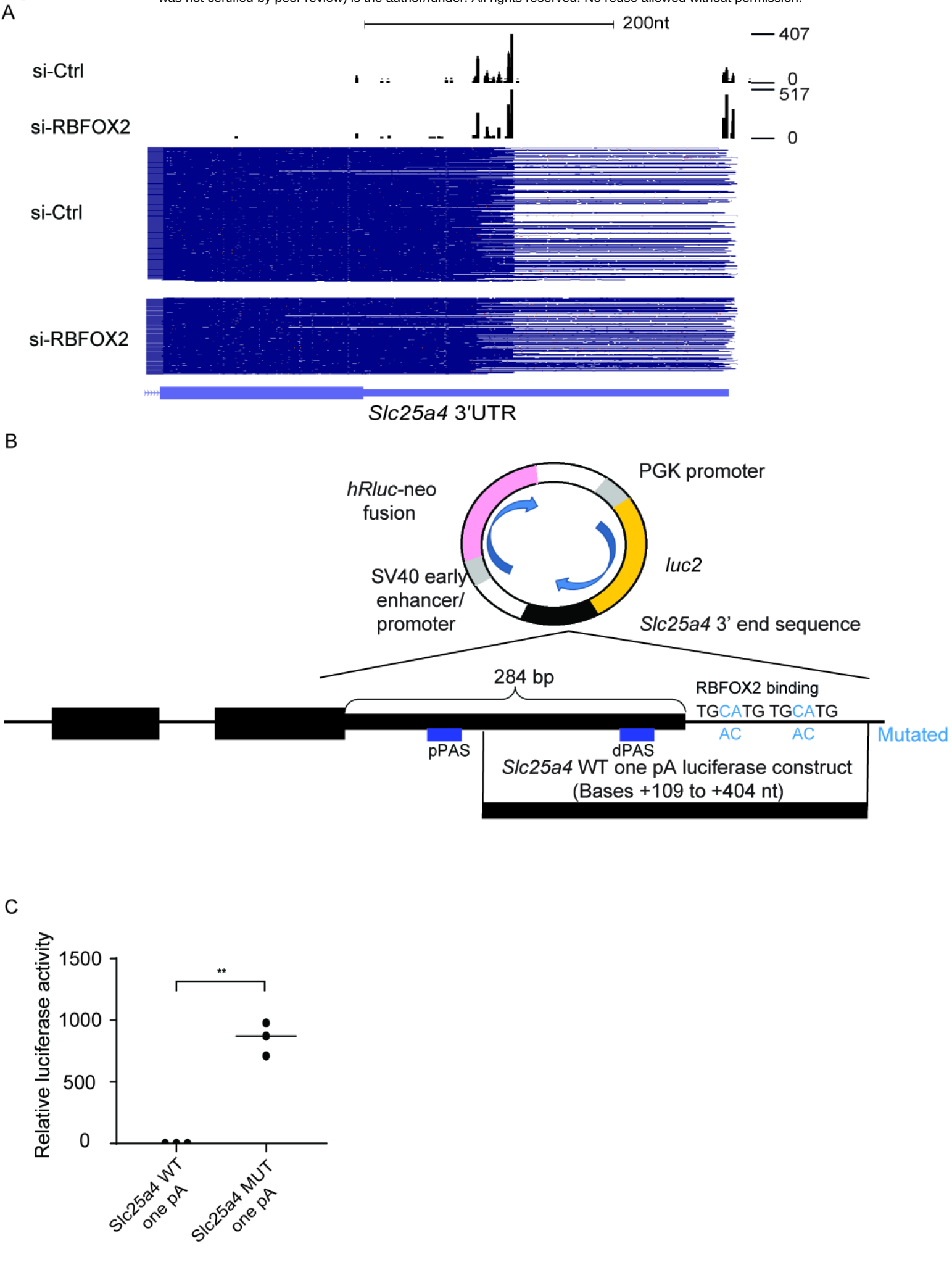

Figure5

A

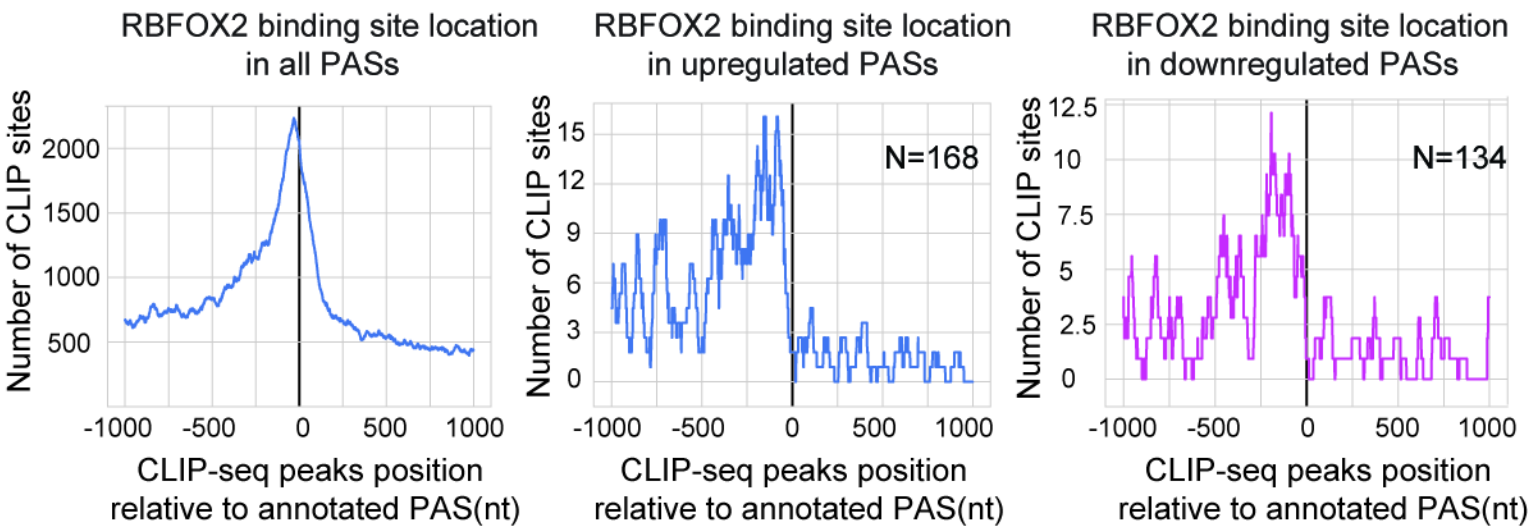

B

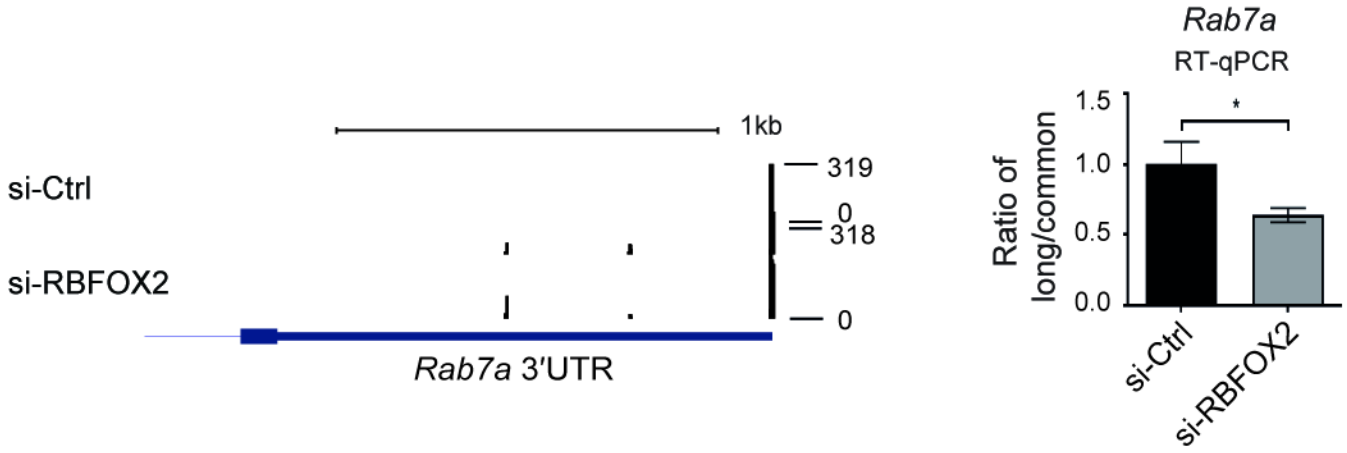

C

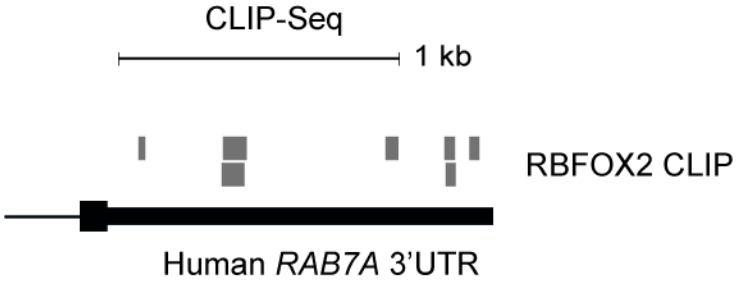

D